JOURNAL OF PROPULSION AND POWER
Vol. 23, No. 4, July–August 2007

Combustion of Nanoscale Al/MoO_3 Thermite in Microchannels

S. F. Son,* B. W. Asay,† and T. J. Foley†
Los Alamos National Laboratory, Los Alamos, New Mexico 87545
and
R. A. Yetter,‡ M. H. Wu,§ and G. A. Risha¶
Pennsylvania State University, University Park, Pennsylvania 16802

DOI: 10.2514/1.26090

Microscale combustion is of interest in small-volume energy-demanding systems, such as power supplies, actuation, ignition, and propulsion. Energetic materials can have high burning rates that make these materials advantageous, especially for microscale applications in which the rate of energy release is important or in which air is not available as an oxidizer. In this study we examine the combustion of mixtures of nanoscale aluminum with molybdenum trioxide in microscale channels. Nanoscale composites can have very high burning rates that are much higher than typical materials. Quartz and acrylic tubes are used. Rectangular steel microchannels are also considered. We find that the optimum mixture ratio for the maximum propagation rate is aluminum rich. We use equilibrium calculations to argue that the propagation rate is dominated by a convective process where hot liquids and gases are propelled forward heating the reactants. This is the first study to report the dependence of the propagation rate with a tube diameter for this class of materials. We find that the propagation rate decreases linearly with $1/d$. The propagation rate remains high in tubes or channels with dimensions down to the scale of 100 μm, which makes these materials applicable to microcombustion applications.

I. Introduction

MESO- or microscale (millimeter length scale and below) combustion has been considered as a potential application in many small-volume, energy-demanding systems, such as power supplies for portable devices, actuation, propulsion for small spacecraft, etc. With large energy densities (~50 MJ/kg), combustion-based micropower devices can be competitive with the energy density of contemporary lithium batteries (~0.6 MJ/kg), at even low overall efficiencies [1]. Energetic materials have a relatively lower chemical energy potential (as low as ~5 MJ/kg for some propellants) [2] compared with hydrocarbon fuels; however, their burning rate can be far superior to many hydrocarbons making them appealing for some applications. Fast propagation rates can result in better combustion efficiency and smaller quench diameters (length scales). The combustion of energetic materials (EMs) in microscale channels has been referred to as either micropyrotechnics [3] or microenergetics [4]. Because of potential advantages, there is a growing interest in applying energetic materials in microscale applications [1–17]. Applications include thrust, actuation (including injection or moving fluids), ignition, power, welding, and rapid switching. The fast reaction rate (deflagration or detonation) of some EMs is an advantage for minimizing heat losses, which is one of the most challenging issues to be solved in microsystems. Fuel tanks, valves, and pumps may be eliminated or reduced in microscale devices using solid EMs, resulting in simpler systems.

Often EMs commonly used for macroscale applications are not ideal for microscale applications. For example, HMX (a high performance EM) deflagration will quench in steel tubes several millimeters in diameter at atmospheric pressures. Even the detonation failure diameter is greater than a millimeter for HMX-based plastic bonded explosives. Consequently, HMX would not be expected to work well in most microenergetic applications. Many other common EMs would also be difficult to ignite, quench after ignition, or have low combustion efficiency. There is a need to consider materials that may have properties that are more ideally suited for microscale applications. Nanoscale energetic composites (also called metastable intermolecular composites or MIC) exhibit extremely fast reactions and propagation rates [18–24]. Consequently, nanoscale composites could have advantages over other materials in microenergetics applications. Tappan et al. [4] performed the first experiments with nanocomposite EMs in microchannels. Recently Tappan successfully propagated these materials in channels as small as 300 × 100 μm.** Several other EMs were also evaluated by Tappan and coworkers. However, the propagation rate was not determined as a function of the size of the microchannel. The aim of this work is to quantify the propagation rate for an optimized mixture for a variety of sizes of microchannels, in both circular and rectangular cross sections. In addition, a more complex geometry with lateral channels was considered to further demonstrate the applicability of these materials to microenergetic applications.

II. Experimental

The materials used in this study were mixtures of nanoscale Al and MoO_3. Spherical nanoaluminum (nominally 79 nm, 81% active Al content) was obtained from NovaCentrix, Corp. (Austin, Texas) with a surface area of 26.5 m^2/g. The MoO_3 used was obtained from Technanogy L.L.C. (Irvine, California) with a surface area of 64 m^2/g, and has a sheetlike morphology with typical dimensions of about 30 × 200 nm. Hexane was used as the solvent in the sonication mixing. In this study, 0.25 g batches of reactants were used with about 10 ml of hexane. Following sonication, the mixtures were placed onto a steel pan and allowed to dry on a hot plate at ~40°C. [Note: These are experimental materials and care should be exercised when handling the composites because of their sensitivity to impact,

Received 22 June 2006; revision received 29 March 2007; accepted for publication 29 March 2007.

*Technical Staff Member, High Explosives Science and Technology, MS C920; currently at Purdue University, West Lafayette, IN 47907. AIAA Member.
†Technical Staff Member, High Explosives Science and Technology.
‡Professor, Department of Mechanical and Nuclear Engineering.
§Graduate Student, Department of Mechanical and Nuclear Engineering.
¶Assistant Professor, Department of Mechanical and Nuclear Engineering; Currently at Penn State Altoona.

**Tappan, A. S., personal communication, Albuquerque, NM, 2006.

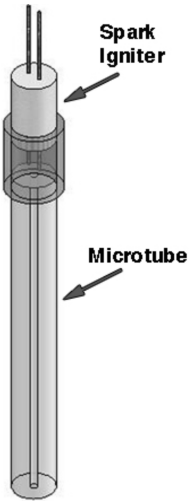

Fig. 1 Schematic of tube experiments. The largest tube used was acrylic. The smaller tubes were borosilicate glass thick-walled capillary tubes. A rubber sleeve holds the igniter near the top of the microtube, as shown.

spark, and friction. Very small samples (<1 g) should be handled and appropriate mitigation used.]

Two experimental configurations were used. Figure 1 is a schematic of the microtube experiment. Thick-walled capillary tubes (borosilicate glass) were used for the three smallest sizes (inner diameters of 0.48, 1.01, and 1.85 mm) and an acrylic tube was used for the largest tube (inner diameter of 3.63 mm). A small section of rubber tube held a spark igniter at the top of the tube (Fig. 1). A small spark ignited the material. These materials require very little ignition energy, which is an advantage in microscale applications. Vibration was used to fill the tubes with Al/MoO_3 powder. The density of the mixture was about 0.35 g/cm^3 or about 9% of theoretical maximum density (TMD). For Al/MoO_3, the TMD is 3.81 g/cm^3. A small amount of the composite is placed on the top of the tube in the rubber tube. Figure 2 shows the configuration for slot experiments. Stainless steel sheets were cut using electrical discharge machining (EDM). The slots were sandwiched in a holder, as shown in Fig. 2, with poly (methyl methacrylate) windows. Figure 3 shows magnified views of two of the slots. The walls appear to have a rough surface. A Phantom 5.1 (Vision Research, Inc.) high-speed video camera was used to monitor the reaction progress. The camera record was triggered by light emission using a photodiode.

III. Results and Discussion

To determine the optimal mixture ratio for fastest propagation, we varied the ratio of nanoaluminum (nAl) to MoO_3. Thick-walled 1.85 mm inside diameter tubes were used. The stoichiometric mass fraction of nAl, accounting for the initial oxide, is 31.6% nAl with 68.4% MoO_3 by weight. As seen in Fig. 4a, the maximum propagation velocity occurs near 38% nAl and 62% MoO_3 by weight. It is not unusual for fuel-rich thermite mixtures to have higher propagation velocities [20], but explanations for this have not been adequate. If stoichiometric portions were used, the propagation velocity decreases by more than 10% from the maximum. In addition, the temperature is predicted to be much lower (over 800 K) at the maximum propagation velocity compared to the stoichiometric ratio. Consequently, if temperature is more important than propagation in a particular application, a stoichiometric ratio may be preferred. In addition, some applications such as thrust demand even higher gas production. This could be accomplished by the addition of gas generants or by choosing other reactants. Our goal here is not to direct this material to any particular application, but to study the effect of diameter on the propagation.

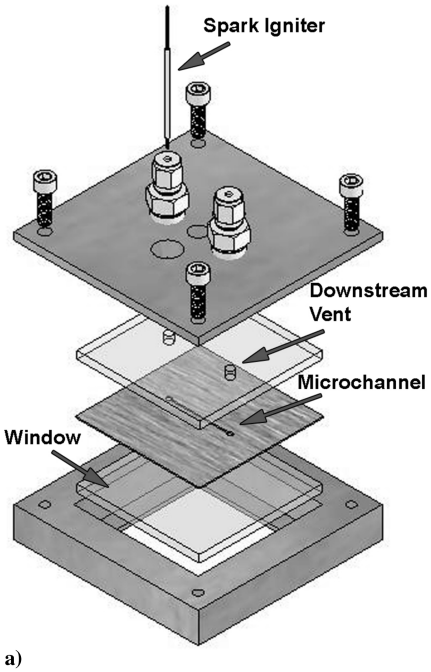

a)

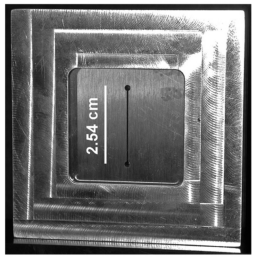

b)

Fig. 2 a) Exploded schematic of the slot experiments. A photograph of the experiment is shown in b).

A. Equilibrium Calculations

To explore the question of why the optimum propagation rate was obtained with a fuel-rich mixture, chemical equilibrium calculations were performed. The Cheetah 4.0 program was used [25]. A constant one-atmosphere pressure problem was considered. The air within the powder is neglected. Including air would change the results very little. For example, including air in a stoichiometric calculation of Al/MoO_3 composite changes the calculated temperature by less than 1%. A further justification for neglecting the air is that the propagation rate in a vacuum or air has been observed to be nearly the same for at least the Al/MoO_3 composite [18].

In a recent paper, Hobbs and Baer [26] reviewed various product libraries and developed the JCZS (Jacobs–Cowperthwaite–Zwisler–Sandia) product library. Using the JCZS product library included in Cheetah 4.0 we found that for very fuel-rich cases solid Al was produced in the products, although the temperature was far above the melting temperature of Al (933 K). This is not physically plausible. Both BKWS (Becker–Kistiakowsky–Wilson–Sandia) and JCZS product libraries produced similar results. The product library EXP6.2 [25] does not predict solid Al forming above the melting temperature. Using the product library EXP6.2 the maximum gas production (mainly Al vapor) corresponds closely to the ratio for peak propagation velocity (near 38% nAl). It appears that gas production is more critical in the reaction propagation than adiabatic temperature. This suggests that convective processes may be important in the propagation. However, EXP6.2 does not include many aluminum species, such as Al_2O, AlO, and others. In addition, EXP6.2 does not predict the solidification of Mo even though predicted temperatures dropped below the melting temperature of Mo (2896 K). Consequently, we did not present the results calculated using the EXP6.2 product library. We were able to obtain a correctly

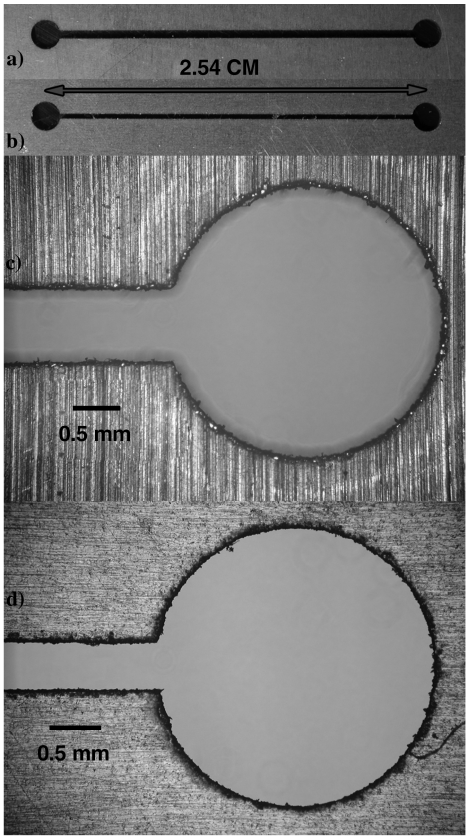

Fig. 3 a), c) Example photographs of the wider steel slots used. b), d) Examples of the narrower slots.

implemented version of the JCZS product library from Mel Baer at the Sandia National Laboratory that does not predict anomalous solid aluminum at temperatures above the melting temperature of aluminum described above. We have compared these calculations with NASA's CEA equilibrium code and predicted adiabatic temperatures are within about ~200 K for the mixtures considered.

We used the JCZS [25,26] product library (Baer's corrected version) in the calculations presented in Fig. 4b. Using the BKWS product library instead would not change the conclusions. At about 39% nAl by weight, solid Mo begins to be predicted in the equilibrium products. This is consistent with the melting temperature of Mo at 2896 K. The knee in the temperature profile near 39% nAl is due to the Mo phase change in the products. At higher mass fractions of nAl, the amount of liquid Mo drops quickly. In contrast to the EXP6.2 calculations, the total gas production does not peak near 38% nAl but continues to rise over the range considered. The amount of liquid Mo peaks near stoichiometric conditions. These results suggest that liquid Mo in the products combined with higher gas production accelerate the propagation, even more than higher temperatures. The mechanism suggested is liquid Mo being propelled forward by hot convective gases and solidifying on unreacted materials. This could be a very effective heat transfer mechanism.

B. Tube Experiments

We chose to consider the mixture ratio resulting in the fastest propagation because this may minimize heat losses. Four tube diameters were considered. A framing rate of 88,888 fps with a shutter time of 3 μs was used. The aperture was adjusted between experiments to keep the exposure adequate. The intensity increased with diameter, as expected. Figure 5 shows a snapshot of four experiments with various diameters. There are no significant differences in appearance.

Figure 6 shows a time sequence for a typical tube (2 mm diam) experiment. There is a short initial transient, followed by propagation

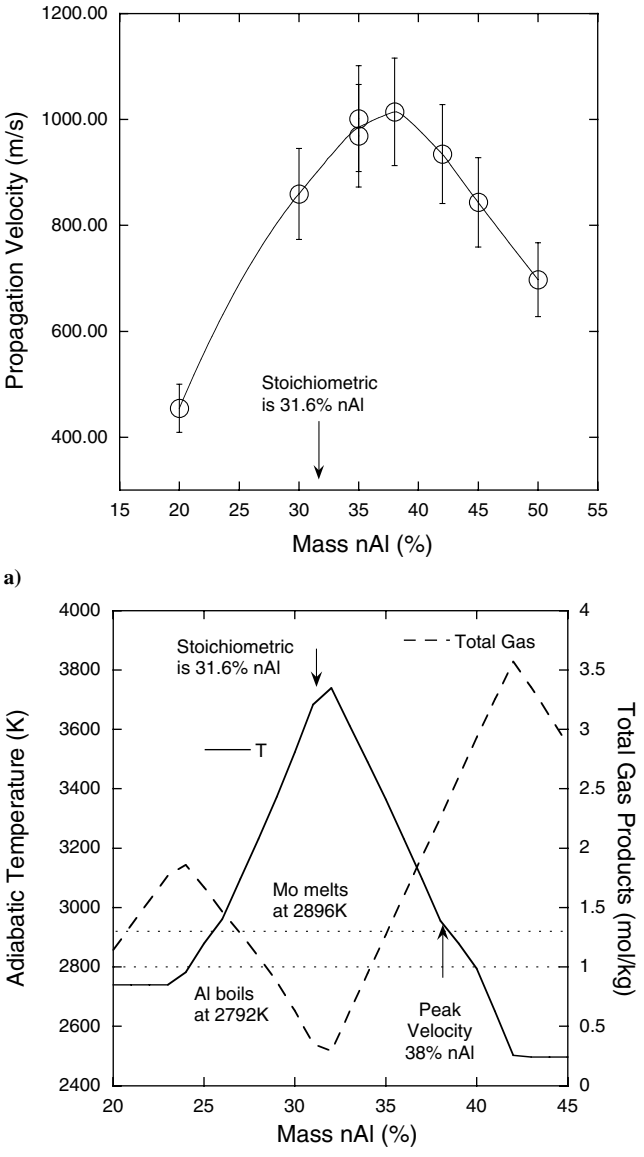

Fig. 4 a) Measured propagation rate as a function of the mass fraction of nAl (%). b) Calculated adiabatic temperature and total gas products.

that appears steady. The expansion of the rubber tube used to hold the spark igniter and some blowby of products from the ignition event is seen near the top of the image.

Decreasing the diameter results in a slower propagation velocity. Figure 7 shows the propagation velocity as a function of diameter for the tubes considered. The uncertainty is very conservatively estimated to be about 10%. Density variations of the powders could introduce the most significant uncertainties. The speed appears to be approaching a limit as the losses to the walls become negligible with larger diameters. Heat or momentum losses to the walls are the likely cause of the slower propagation. This functional dependence is similar to unconfined explosive rate stick results [27]. In high explosives the divergence of the expanding downstream flow reduces the energy available to propagate the detonation.

The propagation speed can also be plotted as a function of the inverse of the diameter d (Fig. 8). For unconfined explosives having large diameters, a linear dependence is observed for unconfined explosives followed by a more rapid drop in detonation velocity [28]. Because the tube walls are not deflected significantly in these experiments as the reactive wave propagates, the loss mechanism is not likely the same as high explosives. However, we see in Fig. 8 that these results produce a linear dependence on $1/d$ for the diameters considered. This may indicate that the failure diameter is far less than

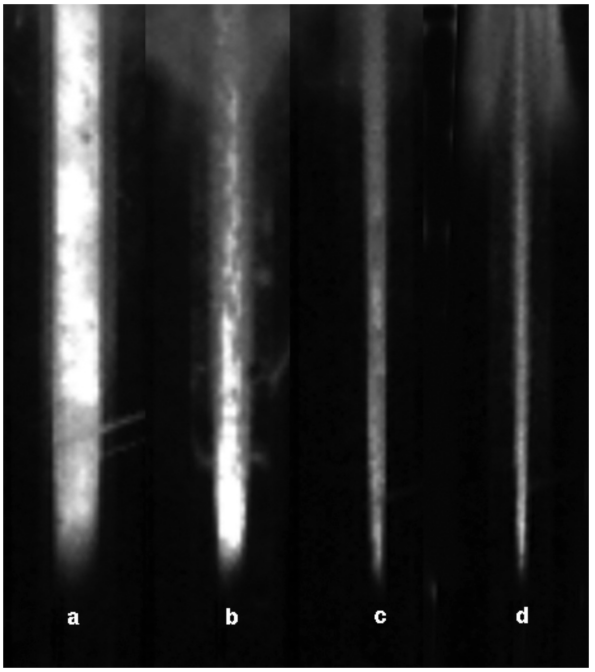

Fig. 5 Single frame images from experiments in the four different diameters used.

the smallest tube used. The linear regression, $V = V_\infty - a/d$, is shown in Fig. 8. The maximum available energy is proportional to the volume, or the cross sectional area on a per length basis. The energy lost by heat transfer or viscous loss is proportional to the surface area, or perimeter in specific terms. The ratio of the energy lost to available energy for propagation would then be proportional to $1/d$. It is not obvious why this effect on propagation rate would be a simple relationship, such as a linear dependence as it appears. The wall losses become negligible as d becomes large. For infinite diameter, the fit extrapolates to a value of 1090 m/s for V_∞. This result shows that larger tubes would not produce much of an increase in propagation speed beyond the largest diameter considered here.

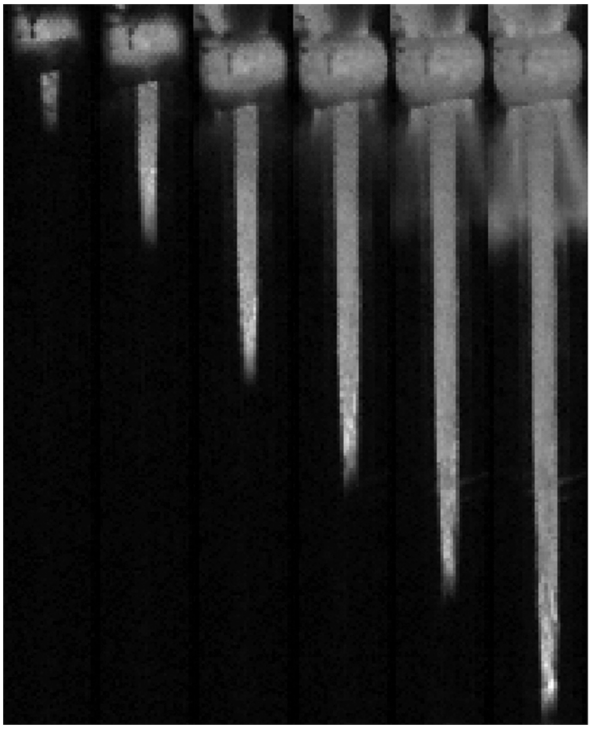

Fig. 6 Image sequence of a single tube experiment. The time between images is 13.8 μs.

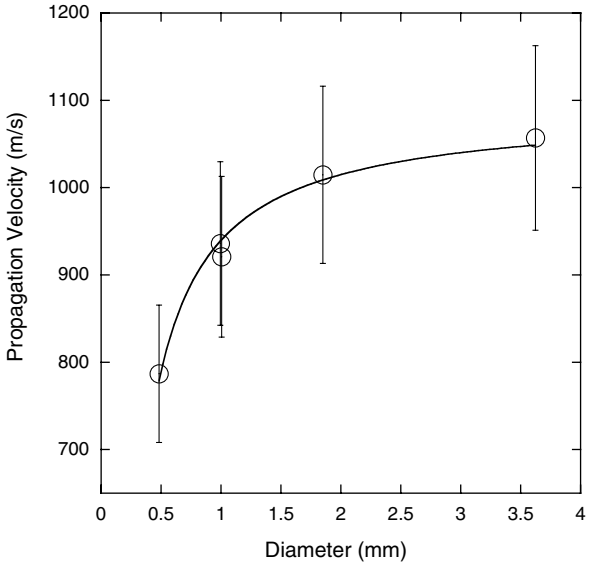

Fig. 7 Propagation velocity as a function of tube diameter.

The parameter a is a material property with units of m^2/s that is expected to change for different materials and initial conditions, such as density and temperature. The ratio $\xi = a/V_\infty$ is a material dependent length scale. For explosives ξ is roughly correlated to the failure diameter [27,28]. Consequently, ξ may be a useful way to compare materials for use in microenergetic applications. Specifically, materials with smaller a and large V_∞ (smaller ξ) would be expected to have smaller failure diameters, and likely better combustion efficiency too. The length scale of this material (ξ), under these conditions, is on the order of 100 nm using the measured results. This is on the same order as the size of the particles used. Explosive failure diameters are on the order of 10ξ [27]. If this also holds for the materials considered here, then the failure diameter for this material would be estimated to be on the order of 1000 nm or 1 μm. It is impossible to load these materials in 1 μm channels. However, if a similarly sized and reactive nanoscale material were assembled in some manner, reaction on the micron scale may be possible. Perhaps smaller failure diameters would be possible for even finer scaled materials. In any case, measuring ξ for different materials and configurations (such as density) of interest could prove to be a very useful way to rank materials for their application in microenergetics.

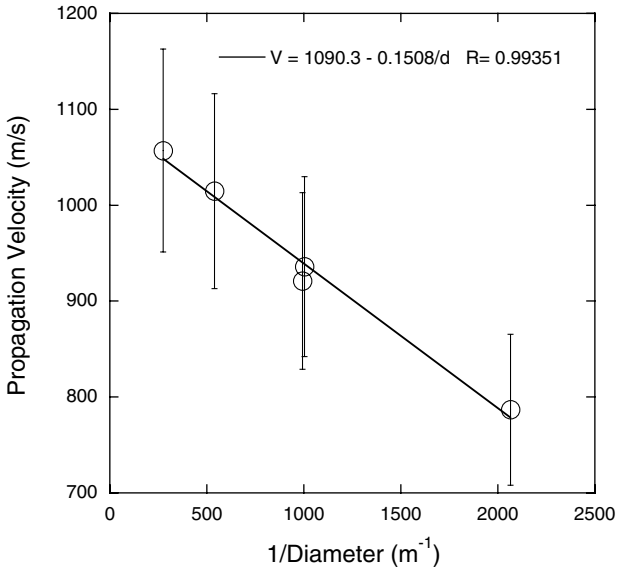

Fig. 8 Propagation velocity as a function of inverse diameter.

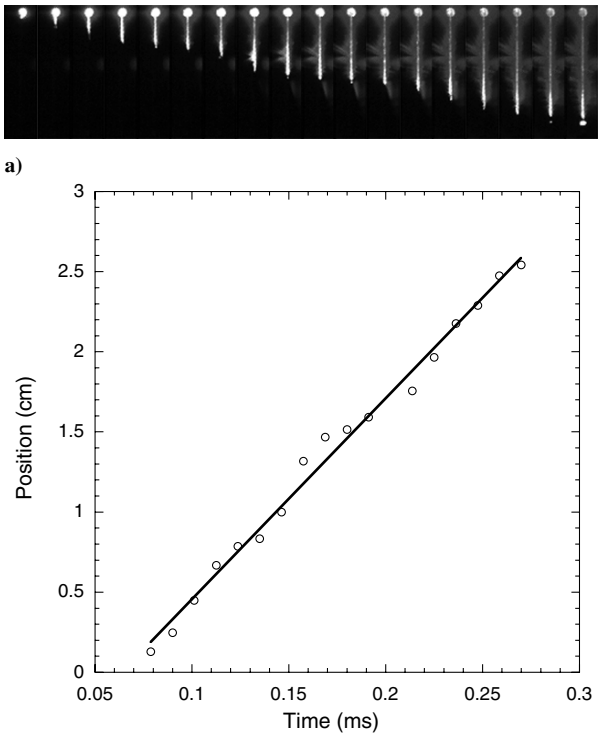

Fig. 9 a) Sequence of images from the smallest slot measured. Time difference between images is 11.3 μs. b) The position as a function of time for the ignition front.

C. Steel Microchannels

In addition to the glass and acrylic tubes, stainless steel slots were investigated. Two widths were considered, 487 and 299 μm. Depths for the 487 μm width slots were 508, 1016, 1397, and 1829 μm. Corresponding hydraulic diameters are 497, 658, 722, and 769 μm, respectively. Depths for the 299 μm slots were 76.2, 177.8, 330.2, 508, 812.8, and 1016 μm. Corresponding hydraulic diameters are 121, 223, 314, 376, 437, and 462 μm, respectively. Figure 9a shows a sequence of images obtained for the smallest slot considered (hydraulic diameter of 121 μm). Unsteady propagation was observed in the two smallest sizes considered. The other results were remarkably steady for such short slots (25.4 mm). Figure 9b shows the position-time location of the ignition front of the smallest slot. The unsteadiness is clearly seen. Figures 10 and 11 summarize the slot results. With the exception of the two smallest hydraulic diameters the data are qualitatively similar to the tube results. It was difficult to pack the two smallest slots with the composite because the small depths makes it difficult to obtain a continuous fill of material, and this may have significantly affected the results. Also, as mentioned above, the flame propagation was not steady. The rest of the data are shifted down to lower velocities compared to the tube data. There are several reasons this may be the case. The walls of the steel slots are much rougher than the acrylic and glass tubes and this could increase the heat and momentum loss to the walls. In addition, the difference in thermal conductivity of the steel from the tubes could contribute to the observed differences, but this should be examined by changing materials in the same configuration in future work. Also, there is some leakage of gases between the steel and windows, as can be seen in Fig. 9 and this would be an additional loss. Moreover, the shorter slot lengths may not have allowed a

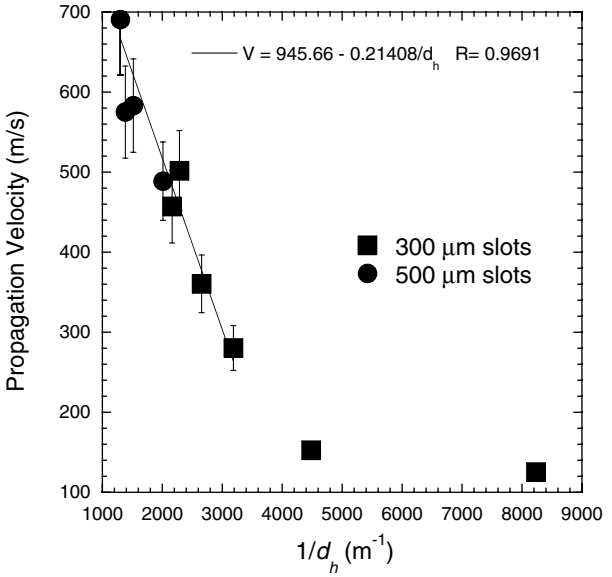

Fig. 11 Propagation velocity as a function of the inverse of hydraulic diameter. Uncertainties are not estimated for the smallest slots because these may be much higher than other experiments and not easy to estimate.

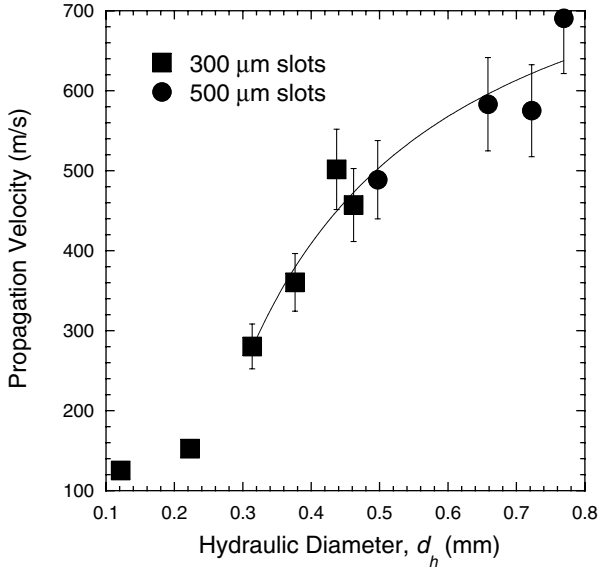

Fig. 10 Propagation velocity of the steel slots. Uncertainties are not estimated for the smallest slots because these may be much higher than other experiments and not easy to estimate.

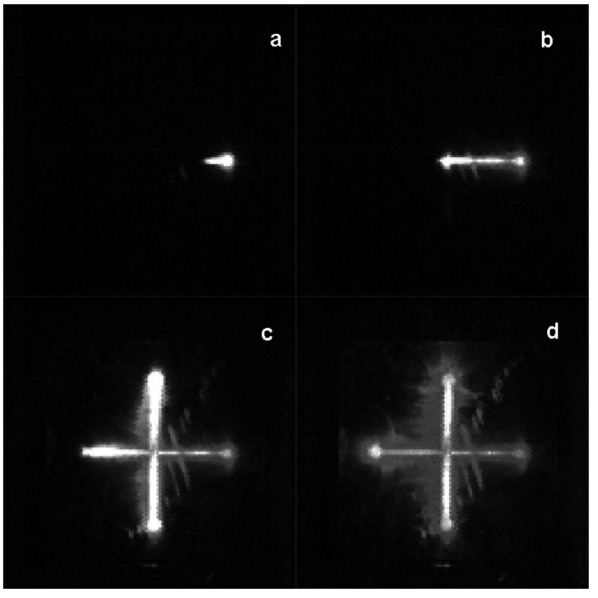

Fig. 12 Image sequence from experiment in connected slots. The time between images is 29.3 μs. The slots are each 25.4 mm long.

propagating flame to become fully developed. It is also possible that the rectangular shape does not appropriately scale to the hydraulic diameter. Nevertheless, the parameter measuring ξ is on the same order of magnitude as obtained for the tubes and the implications are the same for the slots as the tubes.

D. Connected Slots

Some possible applications may require turns or other more complex geometries. Figure 12 shows a more complex slot configuration consisting of a small slot crossing a larger slot using the same two slot sizes considered above. The small slot ignites the wider slots and propagation then proceeds much faster than in the thinner slot demonstrating that the reaction wave can readily turn corners.

IV. Conclusions

In this paper we have examined the applicability of a nanoscale thermite in microchannels; both tubes and slots were used. We optimized the mixture ratio for propagation speed and found that it optimized at a fuel-rich ratio. We performed equilibrium calculations that showed that the peak propagation velocity occurred where there are more gas products and no solid Mo in the products. This implies that propagation is not dominated by the final temperature, as is expected in normal deflagrations. In addition, this indicates that radiation is not the dominant mechanism [18]. Instead, we propose that the propagation is dominated more by hot gas products that propel liquid Mo forward and transfer heat via convection and the solidification of the liquid Mo.

We measured the propagation of the optimized material in smooth walled tubes as a function of diameter. We found that the propagation velocity decreases linearly with inverse diameter, likely controlled by wall losses (heat transfer or viscous effects). Steel slots with two widths and several thicknesses were also considered, extending to a hydraulic diameter of 121 μm. The propagation velocity also decreases linearly with inverse hydraulic diameter for all but the smallest two slots. The propagation velocity in even the smallest slots is near 100 m/s. Classical energetic material would have difficulty igniting and propagating in these small tubes and slots. These results show that nanoscale thermites can ignite and propagate well in microchannels. Consequently, these materials may have applications in various microenergetic (or micropyrotecnic) applications.

These results show that the nanoscale composites such as those considered here may be successfully applied in nanoenergetic applications in very small channels (on the order of at least 100 μm) and are likely limited by much smaller scales. In addition, the improved understanding gained may help in the choice of materials for microenergetic applications.

Acknowledgments

This work was sponsored by the U.S. Army Research Office under the Multi-University Research Initiative under Contract No. W911NF-04-1-0178. The support and encouragement provided by David Mann and Kevin L. McNesby are gratefully acknowledged. S. F. Son, T. J. Foley, and B. W. Asay are supported by the Los Alamos National Laboratory (LANL), which is operated by the University of California for the U.S. Department of Energy under the Contract W-7405-ENG-36.

References

[1] Fernandez-Pello, A. C., "Micropower Generation Using Combustion: Issues and Approaches," *Proceedings of the Combustion Institute*, Vol. 29, No. 1, 2003, pp. 883–899.

[2] Rossi, C., Esteve, D., and Mingues, C., "Pyrotechnic Actuator: A New Generation of Si Integrated Actuator," *Sensors and Actuators A-Physical*, Vol. 74, Nos. 1–3, 1999, pp. 211–215.

[3] Rossi, C., and Esteve, D., "Micropyrotechnics, a New Technology for Making Energetic Microsystems: Review and Prospective—Review," *Sensors and Actuators A-Physical*, Vol. 120, No. 2, 2005, pp. 297–310.

[4] Tappan, A. S., Long, G. T., Renlund, A. M., and Kravitz, S. H., "Microenergetic Materials—Microscale Energetic Material Processing and Testing," AIAA Paper 2003-242, Jan. 2003.

[5] Rossi, C., Scheid, E., and Esteve, D., "Theoretical and Experimental Study of Silicon Micromachined Microheater with Dielectric Stacked Membranes," *Sensors and Actuators A-Physical*, Vol. 63, No. 3, 1997, pp. 183–189.

[6] Rossi, C., Esteve, D., Temple-Boyer, P., and Delannoy, G., "Realization, Characterization of Micro Pyrotechnic Actuators and Fem Modelling of the Combustion Ignition," *Sensors and Actuators A-Physical*, Vol. 70, Nos. 1–2,1998, pp. 141–147.

[7] Rossi, C., Temple-Boyer, P., and Esteve, D., "Realization and Performance of Thin Sio2/Sinx Membrane for Microheater Applications," *Sensors and Actuators A-Physical*, Vol. 64, No. 3, 1998, pp. 241–245.

[8] Rossi, C., Do Conto, T., Esteve, D., and Larangot, B., "Design, Fabrication and Modelling of MEMS-Based Microthrusters for Space Application," *Smart Materials and Structures*, Vol. 10, No. 6, 2001, pp. 1156–1162.

[9] Stewart, D. S., "Towards the Miniaturization of Explosive Technology," *Shock Waves*, Vol. 11, No. 6, 2002, pp. 467–473.

[10] Tappan, A. S., Renlund, A. M., Long, G. T., Kravitz, S. H., Erickson, K. L., Trott, W. M., and Baer, M. R., "Microenergetic Processing and Testing to Determine Energetic Material Properties at the Mesoscale," *Proceedings of the 12th International Detonation Symposium*, Naval Surface Warfare Center, Indian Head, MD, 2002, pp. 3–10.

[11] Larangot, B., Rossi, C., Esteve, D., and Orieux, S., "Solid Propellant Micro Thrusters for Space Application," *Houille Blanche-Revue Internationale De L Eau*, Vol. 5, 2003, pp. 111–115.

[12] Ali, A. N., Son, S. F., Hiskey, M. A., and Nau, D. L., "Novel High Nitrogen Propellant Use in Solid Fuel Micropropulsion," *Journal of Propulsion and Power*, Vol. 20, No. 1, 2004, pp. 120–126.

[13] Zhang, K. L., Chou, S. K., and Ang, S. S., "Development of a Solid Propellant Microthruster with Chamber and Nozzle Etched on a Wafer Surface," *Journal of Micromechanics and Microengineering*, Vol. 14, No. 6, 2004, pp. 785–792.

[14] Zhang, K. L., Chou, S. K., and Ang, S. S., "MEMS-Based Solid Propellant Microthruster Design, Simulation, Fabrication, and Testing," *Journal of Microelectromechanical Systems*, Vol. 13, No. 2, 2004, pp. 165–175.

[15] Rossi, C., Larangot, B., Lagrange, D., and Chaalane, A., "Final Characterizations of MEMS-Based Pyrotechnical Microthrusters," *Sensors and Actuators A-Physical*, Vol. 121, No. 2, 2005, pp. 508–514.

[16] Tappan, A. S., Long, G. T., Wroblewski, B., Nogan, J., Palmer, J. A., Kravitz, S. H., and Renlund, A. M., "Patterning of Regular Porosity in PETN Microenergetic Material Thin Films," *Proceedings of the 36th International Annual Conference of ICT*, Fraunhofer-Institut fur Chemische Technologie (ICT), Berghausen, Germany, 2005.

[17] Zhang, K. L., Chou, S. K., and Ang, S. S., "Development of a Low-Temperature Co-Fired Ceramic Solid Propellant Microthruster," *Journal of Micromechanics and Microengineering*, Vol. 15, No. 5, 2005, pp. 944–952.

[18] Asay, B. W., Son, S. F., Busse, J. R., and Oschwald, D. M., "Ignition Characteristics of Metastable Intermolecular Composites," *Propellants, Explosives, and Pyrotechnics*, Vol. 29, No. 4, 2004, pp. 216–219.

[19] Aumann, C. E., Skofronick, G. L., and Martin, J. A., "Oxidation Behavior of Aluminum Nanopowders," *Journal of Vacuum Science and Technology B, Microelectronics and Nanometer Structures*, Vol. 13, No. 3, 1995, pp. 1178–1183.

[20] Bockmon, B. S., Pantoya, M. L., Son, S. F., Asay, B. W., and Mang, J. T., "Combustion Velocities and Propagation Mechanisms of Metastable Interstitial Composites," *Journal of Applied Physics*, Vol. 98, No. 6, 2005, pp. 064903-1–7.

[21] Pantoya, M. L., Son, S. F., Danen, W. C., Jorgensen, B. S., Asay, B. W., and Busse, J. R., "Characterization of Metastable Intermolecular Composites (MICs)," *Defense Applications of Nanomaterials*, edited by E. A. A. W. Miziolek, Oxford Univ. Press, Oxford, England, U.K., 2004, pp. 227–240.

[22] Perry, W. L., Smith, B. L., Bulian, C. J., Busse, J. R., Macomber, C. S., Dye, R. C., and Son, S. F., "Nano-Scale Tungsten Oxides for Metastable Intermolecular Composites," *Propellants, Explosives, Pyrotechnics*, Vol. 29, No. 2, 2004, pp. 99–105.

[23] Tasker, D. G., Asay, B. W., King, J. C., Sanders, V. E., and Son, S. F., "Dynamic Measurements of Electrical Conductivity in Metastable Intermolecular Composites," *Journal of Applied Physics*, Vol. 99, No. 2, 2006, pp. 23705-1–7.

[24] Moore, K., Pantoya, M. L., and Son, S. F., "Combustion Behaviors Resulting from Bimodal Aluminum Size Distributions in Thermites," *Journal of Propulsion and Power*, Vol. 23, No. 1, 2007, pp. 181–185.

[25] Fried, L. E., Glaesemann, K. R., Howard, W. M., Souers, P. C., and Vitello, P. A., Cheetah 4.0, Lawrence Livermore National Laboratory,

Livermore, CA, 2004.
[26] Hobbs, M. L., Baer, M. R., and Mcgee, B. C., "JCZS: An Intermolecular Potential Database for Performing Accurate Detonation and Expansion Calculations," *Propellants, Explosives, Pyrotechnics*, Vol. 24, No. 5, 1999, pp. 269–279.
[27] Cooper, P. W., "A New Look at the Run Distance Correlation and Its Relationship to Other Non-Steady-State Phenomena," *Proceedings of the 10th Symposium (International) on Detonation*, Naval Surface Warfare Center, Indian Head, MD, 1993, pp. 690–696.
[28] Cooper, P. W., *Explosives Engineering*, Wiley–VCH, New York, 1996, p. 169.

V. Yang
Editor in Chief